

Explicit Dynamic Simulation of Flat Nose Low-Velocity Impact of Relatively Thick Composite Panels Using Built-In Failure Criteria

Umar Farooq, Peter Myler

Department of Engineering, Advanced Sciences, and Support, University of Bolton BL3 5AB, United Kingdom

Abstract— This work reports computational modelling of carbon fibre-reinforced composite panels subjected to flat nose drop-weight impact to predict ply-level failure using built-in failure criteria. It is widely recognised that accidental flat-nose tool (box) drop impact induce internal damage to an aircraft structure during part assembly, maintenance service and operation life. The internal damage remains undetected during routine inspections. However, the damage might cause unexpected catastrophic failure that is a major concern to aircraft industry. Extensive studies are underway on the topic to save human lives as well as capital assets by mitigating detrimental effects of the damage. Nonetheless, majority of the previous studies are experimental based, analytical studies are too complex, while simulation studies compare performance efficiencies of explicit and implicit dynamic solvers. Moreover, the predicted quantities such as load, velocity, deflection, energy, stress, and strain are further utilisation in relevant failure criteria. Thus efficient model is desired to predict ply-level failure. This study proposes reliable and efficient model consisting of mathematical formulation, ABAQUS™/Explicit software simulation, and use of built-in mode-based failure criteria. Selected results were compared to the data results available in the literature and found in acceptable agreement. The model could be easily modified, extended, and useful to simulate similar further studies.

Keywords— Fibrous composites; Low-velocity drop-weight impact; Explicit and Implicit methods, Mode-base Failure Criteria.

I. INTRODUCTION

Carbon fibre-reinforced composites display better economic values and mechanical properties: high ratios of strength, stiffness to weight, flexibility features to tailor part integration, and buckling resistance essential to structural stability. Thus they are being widely used as structural elements in aerospace industry. The heavier structural assemblies are being replaced by composites to enhanced safety and save fuel consumption. Market for the composites' applications is constantly growing in aerospace, sport, automobile, civil and military applications. The state of the art Boeing™ 787 Dream liner and Airbus™ A350XWB aircrafts mainly consist of carbon fibrous composites up to 50-60% by weight. Breakdown of the major structural parts of Boeing 787 Dream linear built from composite materials and sandwich structures are shown in Figure 1.



Figure 1: Breakdown of materials used in the Boeing 787 Dream liner [1]

Since composites made structural elements are vulnerable to foreign object impacts such as tool (tool box) drops on fuselage and wings of an aircraft that could inflict severe internal damage, reduce compressive strength, and might result in unexpected catastrophic failures during future operations as can be seen from Figure 2.

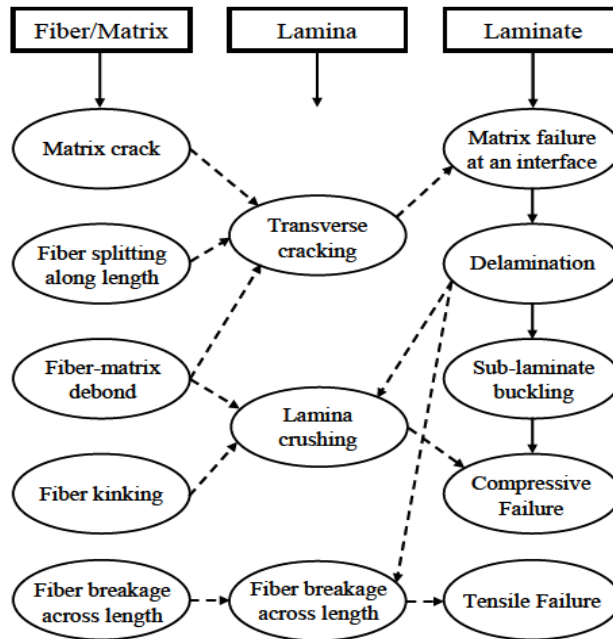


Figure 2: Various failure modes at different scales [1].

To save human lives and structural assets analysis of impact behaviour of composites is required. Investigations of the low-velocity impact performance have received steady attention in the literature. Selected studies are referred below for detailed information. Finite element modelling of low-velocity impact of composite panels was studied in [1] and [2]. A new analytical method was developed for predicting the impact force from the dynamic strain of composite plates subjected to transverse impact in [3]. Analytically and numerically studies on impact resistance modelling of hybrid composite panels revealed effects of different pulse shapes on the impact response [4]. A three-dimensional hybrid stress finite element methods investigated laminated composite plates under dynamic loading in [5]. They modelled the contact force between the projectile and the laminated plate with Hertzian impact law. The contact force on composite plates using impact-induced strain and neural networks was studied in [6]. Response of anisotropic laminated plates to low-velocity impact by a rigid object was predicted in [7]. The contact area was assumed to vary with time, and the complex contact problem was replaced by a loading history that based on available experimental data from the instrumented impact tests. Delamination due to low-velocity impact was investigated in [8]. A new method was proposed for simple prediction of the impact force history on composite laminates subjected to low-velocity impact in [9]. Robust analytical solution technique for the impact response of especially orthotropic rectangular plates was proposed in [10]. Numerical investigations into the response of laminates were carried out using ABAQUS™/EXPLICIT by analysis in [11] & [12]. A new family of explicit time integration methods for linear and non-linear structural dynamics was introduced in [13]. Explicit time integration algorithms for structural dynamics with optimal numerical dissipation were investigated in [14] and [15]. An unconditionally stable explicit method for structural dynamics was proposed in [16]. Performance of an implicit time integration scheme in the analysis of wave propagations is presented in [17], while stress improvement procedure is described in [18]. The finite element method enriched by interpolation covers in [19]. More reliable finite element modelling of linear dynamics problems with the reduced dispersion error is proposed in [25]. Insight into an implicit time integration scheme for structural dynamics is reported in [26]. Comparative study of numerical explicit time integration algorithms is presented in [27]. Comparative study of numerical schemes for impact problems found that the implicit method to be preferable in smaller 2D problems whereas the explicit method is more robust and efficient for complicated models involving contact [28]. Damage and energy absorption behaviour of low-velocity impacted fibre-reinforced composite panels were studied using analytical and data filtering techniques [27]. Stress base modelling and computer simulation of drop-weight impact response of composite panels with domain partitioning and adaptive meshing techniques were studied in [29] and [30]. Validation of a 3D damage model for predicting the response of composite structures under crushing loads. Energy absorption behaviour of low-velocity impacted fibre-reinforced composite panels using analytical and data filtering techniques. Stress base modelling and computer simulation of drop-weight impact response of composite panels with domain partitioning and adaptive meshing techniques [32], [33].

The literature search revealed that most of the studies on the topic are based on efficiency or suitability comparisons of the schemes. Investigations of the ply-level stresses and failures using the schemes are needed.

In this investigation, simulation models were developed for carbon fibrous composite panels subjected to flat nose low-velocity drop-weight impact in ABAQUS™/Explicit software. Simulations produced results for relatively thick laminates 24-Ply panels impacted were selected and compared to predict ply-level failure utilising limits, interactive polynomial, numerical

integrated through-thickness stresses using mode based formulation, and built-in failure criteria. Comparisons of the explicit routine and mode based failure criteria produced results demonstrated that simulation models are capable to predict ply-level failure with different failure mechanisms.

II. FIBRE-REINFORCED COMPOSITE PANELS AND MATERIAL PROPERTIES

The European standard (equivalent to Boeing standard) test laminates consisting of 150 (mm) x 120 (mm) areas were considered. A schematic of 8-Ply symmetric panel with lay-up code $[0/90/45/-45]_S$ is shown in Figure 3(a). All simulated panels were made of aerospace grade carbon fibre-reinforced toughened epoxy code Fibredux 914C-833-40 of material properties given in Table 1. The impact affected circular-area of the laminates consists of central cut-out of diameter 50 (mm), impacted by metallic (steel) round and flat nose impactors as shown at the centre in Figure 3(b). In the simulations, the support is considered perfectly fixed at the edges in conformity with the geometry and boundary conditions defined corresponding to the full-scale test panels.

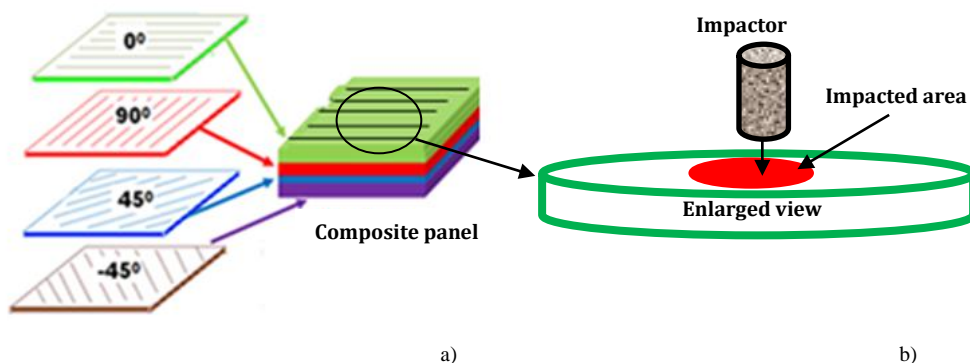


Figure 3: Schematic of a) symmetric composite panel & b) impacted area

Table 1: Material properties of the laminates

Property	Units	Fibredux 914C-833-40
Tensile Modulus (E_{11})	GPa	230
Tensile Modulus ($E_{22}=E_{33}$)	GPa	23
Shear Modulus ($G_{12}=G_{13}$)	GPa	88
Poisson's Ratio (ν_{12})		0.2
Longitudinal Tensile Strength	MPa	1453
Transverse Tensile Strength	MPa	32
Longitudinal Compressive Strength	MPa	650
Transverse Tensile Strength	MPa	15

Since material tested is especially orthotropic and transversally isotropic: the constants are $G_{13} = G_{12}$, $E_2 = E_3$, $\nu_{21} = \nu_{31}$, and $\nu_{23} = \nu_{32}$. In addition, relationship among isotropic engineering constants is associated with the 23 plane, so that

$$G_{23} = \frac{E_2}{2(1+\nu_{32})} \quad (1)$$

Both impactors were made of stainless steel (having a Young's modulus of 210 GPa and Poisson's ratio 0.3) having shank of diameter 20 mm reducing to $10 \pm (0.18)$ mm with the round impactor having a nose shape radius of $5 \pm (0.15)$ mm and flat impactor a ground flat impact face.

III. GOVERNING EQUATIONS AND FINITE ELEMENT FORMULATION OF IMPACT EVENT

Simple fibre-reinforced laminated-plate theories are developed by making assumptions concerning variations of the displacement field in stacks of elastic plies reinforced with fibres oriented at different angles [24]. The laminated-plate consists of stack of layers symmetrical about mid-surface is the building block to determine ply level stress and strain of a structural element. Impact process of panels based on mathematical and physical principles are described in differential equations, while components of the stress and strain tensors are determined solving the differential equations. Determined quantities of strain and stress components are then used in failure criteria to predict ply level failures, optimize residual strength algorithms, and to approximate other impact damage parameters. In drop-weight impact problems applications loads are applied in normal to the plate (in z direction), in-plane, bending or shear to the edges. Such loading produce deformations of the plate in the coordinate directions are characterized by displacements (u, v and w). Dynamic equations for laminated-panel were derived by modifying the static equations using Newton's second law in [20] below. Derivation of formulation steps governing impact-induced deformations in composite-plate from strain-displacement, constitutive, and resultants (forces and moment) relations along with compatibility conditions are detailed in flowchart Figure 4.

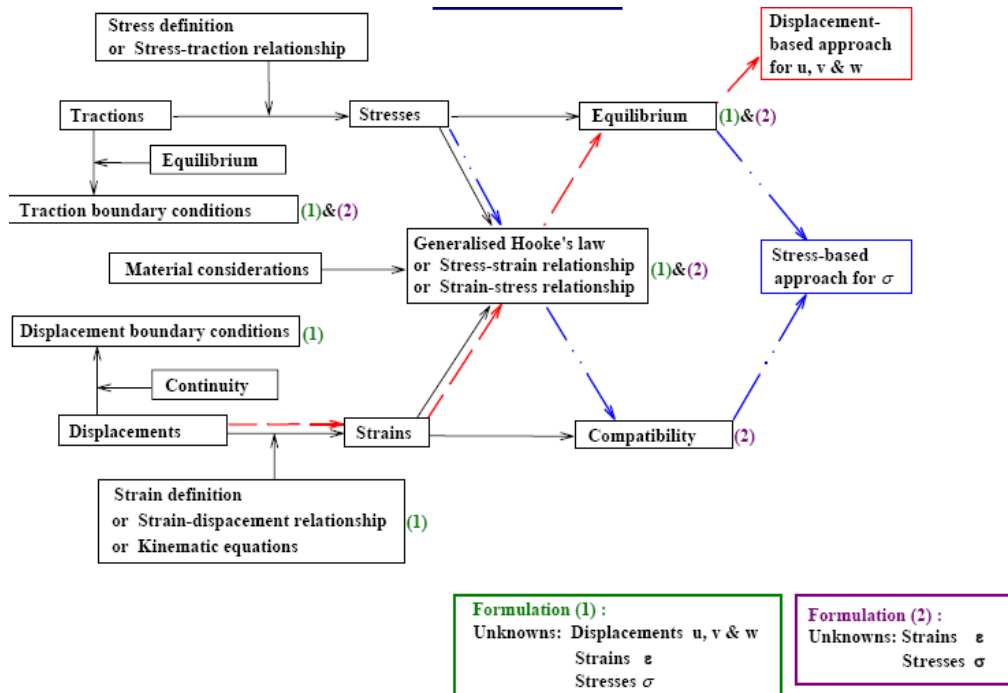


Figure 4: Flowchart of development of governing equations

Accordingly, finite element formulation is developed from the equilibrium equations at instant time in variation form expressed as:

$$\int_v \rho \mathbf{u}_{i,tt} \delta \mathbf{u}_i dv + \int_v \rho \sigma_j \delta \epsilon_j dv - \int_{\partial s} T_i \delta u_i da = \begin{cases} i = 1, 3 \\ j = 1, 3, 5 \end{cases} \quad (2)$$

Where u_i and $u_{i,tt}$ are the displacement and accelerations, respectively. T_i is the contact force distribution during impact. σ_j and ϵ_j are the stresses and strains due to the mechanical loading. For laminated-panels, material properties vary from layer to layer throughout the thickness depending upon the laminate stacking sequence. Thus the variation form may be written as follows:

$$\sum_{n=1}^N [\int_v \rho \mathbf{u}_{i,tt} \delta \mathbf{u}_i dv + \int_v \rho \sigma_j \delta \epsilon_j dv] dh = \int_{\partial s} T_i \delta u_i da \quad (3)$$

Where: N is the total number of the layers in the panel. The subscript forward n indicates the corresponding layer within the panel. Thus, the mechanical stresses in the n^{th} layer are related to the mechanical strains of the corresponding layer through the following equation:

$$\{\epsilon_{11}, \epsilon_{22}, \epsilon_{12}\}^T = \sum_{n=1}^N [C] \{u_{11}, u_{22}, u_{12}\}^T \quad (4)$$

The superscript T means transposition of a vector or a matrix. In order to solve Eq. (2), the distribution of the contact force between the impactor and the impacted laminate has to be known first. The contact force distribution is determined using the Hertzian contact law [22]. Thus, the contact force can be related to the indentation depth α (the distance between the centre of the projectile's nose and the mid-surface of the plate) by the expression

$$F = k \alpha^{3/2} \quad (5)$$

Where k is the modified constant of the Hertz contact:

$$k = \frac{4}{3} \sqrt{r} \left[\frac{1}{(1-\nu_{12}^2)/E_{12} + 1/E_{22}} \right] \quad (6)$$

Where r, ν and E's are the local radius, Poisson's ratio, and the Young's modulus of the impactor respectively. Differential equilibrium may be written in compact form,

$$\sigma_{ij,j} + f_i = \rho \ddot{u}_i \quad (7)$$

The Eq. (7) satisfies traction boundary conditions $\sigma_{ij} n_j = t_i(t)$, and displacement boundary conditions $u_i = D_i(t)$. The weak form of Eq. (7) may be obtained through the principle of virtual work, a simple physical interpretation: the rate of work done by the external forces subjected to any virtual velocity field is equal to the rate of work done by the equilibrating stresses on the rate of deformation of the same virtual velocity field. Multiplying Eq. (7) by an arbitrary vector-valued test function over the entire volume and integrating. The test function can be a velocity field δv that satisfies kinematical constraints and have sufficient continuity. The product of this test function with the equilibrium force field then represents the virtual work rate,

$$\delta \pi = \int \rho \ddot{u}_i \delta v_i dv + \int \sigma_{ij} \delta v_{i,j} dv - \int f_i \delta v_i dv - \int t_i \delta v_i dS \quad (8)$$

Basis for the development of a displacement-interpolation finite element model is the introduction of local spatial approximation written as

$$\mathbf{u} = \mathbf{N}_n \mathbf{u}^n \tag{9}$$

Where N_n are interpolation functions that depend on some material coordinate system and u^n are nodal displacements. Since δv must be compatible with all kinematical constraints, it must have the same spatial variation as the assumed displacements,

$$\delta v = \mathbf{N}_n \delta v^n \tag{10}$$

The internal virtual work, re-written in terms of conjugate pair of stress and strain and the continuum variation statement of Eq. (8) is approximated over the finite set δv^n as

$$\delta v^n (\int \rho \mathbf{N}^T \mathbf{N} d v \ddot{\mathbf{u}} + \int \mathbf{B}^T \boldsymbol{\sigma} d v - \int \mathbf{N}^T \mathbf{f} d v - \int \mathbf{N}^T t d S) \tag{11}$$

As δv^n was chosen to be non-zero, all the other terms in Eq. (11) equate to zero. This in turn arrives at a system of non-linear equations,

$$\int \rho \mathbf{N}^T \mathbf{N} d v \ddot{\mathbf{u}} + \int \mathbf{C}^T \boldsymbol{\sigma} d v - \int \mathbf{N}^T \mathbf{f} d v - \int \mathbf{N}^T t d S \tag{12}$$

The matrix [C] defines strain variation from variations of the kinematical variables is derivable immediately from the interpolation functions once a particular strain measure is to be used. This system forms the basis for the standard assumed displacement finite element procedure,

$$\mathbf{M} = \int \rho \mathbf{N}^T \mathbf{N} d v \tag{13}$$

$$\mathbf{F}_{int} = \int \mathbf{C}^T \boldsymbol{\sigma} d v \tag{14}$$

$$\mathbf{F}_{ent} = \int \mathbf{N}^T \mathbf{f} d v + \int \mathbf{N}^T t d S \tag{15}$$

Arriving at the equation of motion

$$\mathbf{M} \ddot{\mathbf{u}} + \mathbf{F}_{int}(\mathbf{u}) = \mathbf{F}_{ent} \tag{16}$$

This Eq. (16) is solved for u in time. Analytical solutions of the equation of motions are generally not possible if the excitation varies arbitrarily with time or if the system is non-linear, as like drop-weight impact of composite panels. Such problems could be tackled by numerical time-stepping methods for integration of differential equations with either an implicit or an explicit method. Both can be used in static and dynamic analyses, the differences between the methods make them suitable at varying situations.

IV. SELECTION OF NUMERICAL SOLUTION METHODS

Models representing impact damage problems are being solved using either analytical calculations or extensive experimental data. Analytical predictions of the impact damage problems are overly simplified and unreliable. Furthermore, generating data by physical testing for every structural element is time consuming and costly. Finite element based simulations can provide efficient and low cost method to generate similar data through virtual testing for many of the actual impact testing. Once impact event and the damage mechanisms are simulated, progressive failure analyses can be carried out. Hence, promising numerical scheme to solve and predict dynamic response of composite panels due to drop-weight impact over a short-time length was selected from widely used implicit and explicit methods.

4.1 Implicit method

The Implicit method is a general-purpose analysis technique that can solve a wide range of linear and nonlinear problems involving the static, dynamic, thermal, and electrical response of components. Implicit method solves a system of equations implicitly at each solution “increment.” The majority of finite element programs use implicit methods to carry out a dynamic solution of structures subjected to time varying loads including impact loads. Normally, these programs use Newmark schemes to integrate in time and formulation allows pre-assumed static as well as a dynamic approach. In the pre-assumed-static case where acceleration and velocity forces are neglected, the load-displacement leads to Eq. (7) and Eq. (8) for the implicit dynamic case. If the current time step is step ‘n’ an estimate of the acceleration at the end of step $n + 1$ will be $\{\ddot{u}_{n+1}\}$. The Eq. (8) may be written at the next step as:

$$[\mathbf{M}]\{\ddot{u}_{n+1}\} + [\mathbf{C}]\{\dot{u}_{n+1}\} + [\mathbf{K}]\{u_{n+1}\} = \{F_{n+1}\} \tag{17}$$

Where:

\ddot{u}_{n+1} = estimated acceleration at step $n+1$

\dot{u}_{n+1} = estimated velocity at step $n+1$

u_{n+1} = estimated displacement at step $n+1$

F_{n+1} = vector of externally applied loads at step $n+1$, and

Implicit methods are solved in time by applying Newmark method. Considering motion of the impactor, the displacement can be calculated from the standard kinematic using velocity and acceleration:

$$\mathbf{u} = \dot{\mathbf{u}} t + \frac{1}{2} \ddot{\mathbf{u}} t^2 \tag{18}$$

Based on the assumption that the acceleration varies linearly between two instants of time, the resulting expression for the velocity and displacement vectors may be written as:

$$\dot{\mathbf{u}}_{n+1} = \dot{\mathbf{u}}_n + [(1 - \beta)\dot{\mathbf{u}}_n + \beta\dot{\mathbf{u}}_{n+1}]\Delta t \tag{19}$$

$$\mathbf{u}_{n+1} = \mathbf{u}_n + \dot{\mathbf{u}}_n \Delta t + \left[\left(\frac{1}{2} - \alpha\right)\ddot{\mathbf{u}}_n + \alpha\ddot{\mathbf{u}}_{n+1}\right]\Delta t^2 \tag{20}$$

Where the parameters α and β indicate how much the acceleration at the end of the interval enters into the velocity and displacements. The end of the interval Δt can be chosen to obtain the desired accuracy and stability. When $\beta = 1/2$ and $\alpha = 1/6$,

Eqs. (19)-(20) correspond to the linear acceleration method which can also be obtained from Wilson- θ algorithms (scheme when $\theta = 1$). When $\alpha = 1/2$ and $\beta = 1/4$ the Eqs. (18) and (16) corresponds to the constant acceleration between marching steps t_n and t_{n+1} . If displacement is obtained by integration using the mean value theorem then the displacement may be written as:

$$\mathbf{u}_{n+1} = \mathbf{u}_n + \dot{\mathbf{u}} \Delta t + \frac{1}{2} \ddot{\mathbf{u}} \beta \Delta t^2 \tag{21}$$

Where:

$$\ddot{\mathbf{u}}_{\beta} = (1 - 2\beta)\ddot{\mathbf{u}}_n + 2\beta\ddot{\mathbf{u}}_{n+1} \quad 0 \leq \beta \leq 1 \tag{22}$$

Newmark integration parameters become the mid-points ($\alpha = \beta = 1/2$). The Eq. (19) and (20) reduce to:

$$\dot{\mathbf{u}}_{n+1} = \dot{\mathbf{u}}_n + \alpha \ddot{\mathbf{u}}_{n+1} \Delta t \tag{23}$$

$$\mathbf{u}_{n+1} = \mathbf{u}_n + \beta \ddot{\mathbf{u}}_{n+1} \Delta t^2 \tag{24}$$

The Eq. (23) can be utilised to express $\ddot{\mathbf{u}}_{n+1}$ in terms of \mathbf{u}_{n+1} and the resulting expression can be substituted in Eq. (21) to express \mathbf{u}_{n+1} in terms of \mathbf{u}_n . By substituting these expressions for $\dot{\mathbf{u}}_{n+1}$ and $\ddot{\mathbf{u}}_{n+1}$ into Eq. (21) the following relation is obtained for finding displacement:

$$\mathbf{u}_{n+1} = \left[\frac{1}{\alpha(\Delta t)^2} [\mathbf{M}] + \frac{\beta}{\alpha \Delta t} [\mathbf{C}] + [\mathbf{K}] \right]^{-1} \left\{ \mathbf{F}_{n+1} + [\mathbf{M}] \left(\frac{1}{\alpha(\Delta t)^2} \mathbf{u}_n + \frac{1}{\alpha \Delta t} \dot{\mathbf{u}}_n + \left(\frac{1}{2\alpha} - 1 \right) \ddot{\mathbf{u}}_n \right) + [\mathbf{C}] \left(\frac{\beta}{\alpha \Delta t} \mathbf{u}_n + \left(\frac{\beta}{\alpha} - 1 \right) \dot{\mathbf{u}}_n + \left(\frac{\beta}{\alpha} - 2 \right) \frac{\Delta t}{2} \ddot{\mathbf{u}}_n \right) \right\} \tag{25}$$

Number of finite element software use implicit methods to obtain dynamic solution of impacted structures by integrating time step in n interval up to estimate of acceleration at the end of step n + 1. These implicit methods are unconditionally stable; therefore, time step size may be chosen according to the required accuracy. However, solution procedure is complicated with increasing degree of nonlinearities that leads to the inversion of larger matrices, the associated time steps, and larger computing resources.

4.2 Explicit method

The explicit method is suitable for fast dynamic processes and nonlinear analyses such as drop-weight impact simulations. The equilibrium is expressed at an instant when the displacements are known, no equilibrium iterations are needed, and convergence issues that emerge with implicit methods could be avoided. New equilibrium data can be calculated for the next time step. Only known information between the previous time step and the current are used to calculate the equilibrium at next time step. Equation of motion at step i can be written:

$$\mathbf{M} \ddot{\mathbf{u}}_i + \mathbf{C} \dot{\mathbf{u}}_i = \mathbf{F}_i \tag{26}$$

For the next step the equation reads:

$$\mathbf{M} \ddot{\mathbf{u}}_{i+1} + \mathbf{C} \dot{\mathbf{u}}_{i+1} = \mathbf{F}_{i+1} \tag{27}$$

This method is based on finite difference approximation of the time derivatives of displacement ($\dot{\mathbf{u}}_i$ and $\ddot{\mathbf{u}}_i$). Taking the time steps, $\Delta t_i = \Delta t$, the central difference expressions for velocity and acceleration at time i are

$$\dot{\mathbf{u}}_i = \frac{\mathbf{u}_{i+1} - \mathbf{u}_{i-1}}{2\Delta t} \tag{28}$$

$$\ddot{\mathbf{u}}_i = \frac{\mathbf{u}_{i+1} - 2\mathbf{u}_i + \mathbf{u}_{i-1}}{(\Delta t)^2} \tag{29}$$

Substituting these approximate expressions for velocity and acceleration into Eq. (16) gives

$$\mathbf{M} \left(\frac{\mathbf{u}_{i+1} - 2\mathbf{u}_i + \mathbf{u}_{i-1}}{(\Delta t)^2} \right) + \mathbf{C} \left(\frac{\mathbf{u}_{i+1} - \mathbf{u}_{i-1}}{2\Delta t} \right) = \mathbf{F}_i \tag{30}$$

In this equation \mathbf{u}_i and \mathbf{u}_{i-1} are assumed known (from the preceding time step). Transferring these known quantities to the right-hand side leads to

$$\left[\frac{\mathbf{m}}{(\Delta t)^2} + \frac{\mathbf{c}}{2\Delta t} \right] \mathbf{u}_{i+1} = \mathbf{F}_i - \left[\frac{\mathbf{m}}{(\Delta t)^2} - \frac{\mathbf{c}}{2\Delta t} \right] \mathbf{u}_{i-1} - \left[\mathbf{k} - \frac{\mathbf{c}}{2\Delta t} \right] \mathbf{u}_i \tag{31}$$

Thus Eq. (31) gives the solution vector \mathbf{u}_{n+1} once \mathbf{u}_n and \mathbf{u}_{n-1} are known. The method integrates accelerations exactly. The lump mass matrix 'M' is a diagonal which assumes inconsistent structures. Inversion of the matrix is direct and trivial. Therefore, Eq. (30) is a set of independent coefficients. Typically, explicit time steps are orders of magnitude less than those used with implicit codes. The size of a time step or a time increment is of importance in terms of stability demands. If time increment is larger than the time for a dilatational wave to cross any of the elements, errors appear and that can stop the simulation. The mesh density is therefore very important. Smaller element sizes leading to smaller time steps and thus larger number of increments and computational cost. Explicit methods can be made unconditionally stable if the time step is chosen to be less than the time taken for a stress wave to cross the smallest element in the mesh. The finite element equations in the explicit approach are reformulated as being dynamic and in this form they can be solved directly to determine the solution at the end of the increment, without iteration. This may result in reducing considerable computing time it always uses a diagonal matrix hence accelerations computations are trivial without large matrix (only a diagonal matrix), making the nodal calculations computationally inexpensive. Once displacements are found strains and stresses can be determined to predict the load at which failure initiates, and may be compared with the corresponding allowable values employing common failure theories. Since explicit code offers better approach as it allows direct solution and accommodates nonlinearity more easily than implicit methods do. The methods require

little computation time per step, but demand a small time step as they are conditionally stable. Thus the method is best suited to short-duration loads such as drop-weight impact.

V. SELECTION OF FAILURE CRITERIA

Every material has certain strength, expressed in terms of stress or strain, beyond which it fractures or fails. After this point a structural component can no longer support the loads acting on it and fulfill the function for which it was designed. A failure criterion is applied to hypothesize the loading response and failure of a structure. The results are utilised to design structural component, calculate margin of safety, guide in material development, and predict location of weak and strong directions. Numerous failure theories have been proposed which combine features of the various approaches to identify the mode of failure. Failures in metallic materials are characterized by yield strengths. The strength parameter criteria could be applied to validate and compare results from simplified and homogeneous composite materials before rigorous analyses. The commonly applied failure criteria for such materials are: maximum normal stress (Rankine), maximum shear stress (Tresca), maximum normal strain theory (St. Venant), maximum distortional energy (von Mises) criteria. All theories can be expressed in terms of the basic strength parameters referred to the principal material axes stresses, strains, or combination of these that cause onset of yield or failure. The most relevant and selected ones are being presented below.

5.1 Maximum stress criteria (limit theory)

The maximum stress criteria are simple non-interacting failure criteria that compare each stress component against the corresponding material ultimate strength allowable value. The criteria are based on finding the stresses in the local axes and then using five strength parameters to find whether a lamina has failed where each stress component is compared to its allowable value (either tension or compression). If that ratio exceeds unity, then failure initiation has occurred for that stress component at that material point. That is, each component may fail independently at different load levels, and the maximum stress failure. The failure takes on a positive value for tensile-related failures and a negative value for compressive-related values. Shear-related failures have positive values for the failure.

5.2 Maximum strain criteria (energy conservation)

This theory is based on the maximum normal strain theory by St. Venant and the Maximum Shear stress theory by Tresca as applied to isotropic materials. The strains applied to a lamina are resolved to strains in the local axis. Failure is predicted in a lamina, if any of the normal shearing strains in the local axes equal or exceed the corresponding ultimate strain. Given the strains and stresses in an angle lamina the strain in the local axes can be found. The maximum strain criteria are simple non-interacting failure criteria that compare the strain components against the corresponding material ultimate strain allowable value for three-dimensional problems where each strain component is compared to its allowable value (either tension or compression). If that ratio exceeds unity, then failure initiation has occurred for that strain component at that material point, each component may fail independently at different load levels, and the maximum strain failure.

5.3 Interactive polynomial criteria

Adapting the Limits Criteria, failure theories were proposed to account anisotropy in stiffness and strength of the composites. Interacting and quadratic criteria fit well to biaxial loading as long as the two interacting stresses affect the same failure mechanism. When two interacting failure mechanisms are different, such as longitudinal and transverse failures, the quadratic criteria forces an artificially smooth transition from one failure into the other. The widely applied failure criteria are Tsai-Hill and Tsai-Wu. The Tsai-Wu failure criteria were selected to predict ply-by-ply failure employing the simulation generated in-plane stress quantities. The Tsai-Wu failure polynomial is an interacting failure criterion since all stress components are used simultaneously to determine whether a failure at a material point has occurred or not. Identifying the mode of failure requires a different approach for the material degradation step in the progressive failure model from that used with the maximum stress criteria. No distinction is made between tension and compression values for the normal stress components in evaluating the Tsai-Wu failure polynomial terms. The shortcoming of Tsai-Hill and Tsai-Wu criteria is that they do not utilise through-thickness stresses and could not explicitly differentiate matrix failure from fibre failure. To include effects of through-thickness stresses the physical mode based failure criteria were applied.

5.4 Mode-based failure criteria

Failure criteria proposed in limit and inter-active theories are two and three-dimensional and associated with lamina failure and do not include the out of plane stresses and they are very effective for the application of thin structures where out-of-plane stresses are negligible. The proposed 2D unidirectional failure criterion is composed of 'Fibre-Fracture Mode' due to tensile-flexure coupling and 'Quadratic Stress Criterion' for delamination proposed in [24] has been utilised to predict failure and damage of impacted laminates against the strength parameters given in Eqs(32)-(42) below. The inter-active failure criterion (2-D) for unidirectional composite lamina is based on relations for the tensile fibre mode, if $\sigma_{11} > 0$:

$$\left(\frac{\sigma_{11}}{x_T}\right)^2 + \frac{\sigma_{12}}{s_c} \geq 1 \quad (32)$$

For the compressive fibre mode, if $\sigma_{11} < 0$ then

$$\left(\frac{\sigma_{11}}{X_c}\right)^2 \geq 1 \tag{33}$$

For the tensile matrix mode, if $\sigma_{22} > 0$:

$$\left(\frac{\sigma_{22}}{Y_T}\right)^2 + \frac{\sigma_{12}}{S_c} \geq 1 \tag{34}$$

For the compressive matrix mode, if $\sigma_{22} < 0$:

$$\left(\frac{\sigma_{22}}{2S_c}\right)^2 + \left[\left(\frac{Y_c}{2S_c}\right) - 1\right] \frac{\sigma_{22}}{Y_c} + \left(\frac{\sigma_{12}}{S_c}\right)^2 \geq 1 \tag{35}$$

Where: σ_{11} and σ_{22} are the stresses parallel and perpendicular to fibre direction, σ_{12} is the in-plane shear stress of the lamina, X_T is the tensile strength of the fibres, X_C is the compressive strength of the fibre, Y_T is the tensile strength in the transverse direction of the fibres, Y_C is the compressive strength in the transverse direction of the fibres, and S_C is the in-plane shear strength. However, the interactive failure criteria utilised do not include out-of-plane stresses. Hashin proposed a general failure criterion in terms of the stress invariants for a transversely isotropic material in [29]. The failure modes associated with the criteria are:

Tensile fibre failure for $\sigma_{11} \geq 0$

$$\left(\frac{\sigma_{11}}{X_T}\right)^2 + \frac{\sigma_{12}^2 + \sigma_{13}^2}{S_{12}^2} = \begin{cases} > 1 \text{ failure} \\ \leq 1 \text{ no failure} \end{cases} \tag{36}$$

Compressive fibre failure for $\sigma_{11} < 0$

$$\left(\frac{\sigma_{11}}{X_C}\right)^2 = \begin{cases} > 1 \text{ failure} \\ \leq 1 \text{ no failure} \end{cases} \tag{37}$$

Tensile matrix failure for $\sigma_{22} + \sigma_{33} > 0$

$$\left(\frac{\sigma_{22} + \sigma_{33}}{Y_T}\right)^2 + \frac{\sigma_{23}^2 - \sigma_{22}\sigma_{33}}{S_{23}^2} + \frac{\sigma_{12}^2 + \sigma_{13}^2}{S_{12}^2} = \begin{cases} > 1 \text{ failure} \\ \leq 1 \text{ no failure} \end{cases} \tag{38}$$

Compressive matrix failure for $\sigma_{22} + \sigma_{33} < 0$

$$\left[\left(\frac{Y_c}{2S_{23}}\right)^2 - 1\right] \left(\frac{\sigma_{22} + \sigma_{33}}{Y_c}\right) + \frac{(\sigma_{22} + \sigma_{33})^2}{4S_{23}^2} + \frac{(\sigma_{23}^2 - \sigma_{22}\sigma_{33})}{S_{23}^2} + \frac{\sigma_{12}^2 + \sigma_{13}^2}{S_{12}^2} = \begin{cases} > 1 \text{ failure} \\ \leq 1 \text{ no failure} \end{cases} \tag{39}$$

Inter-laminar normal stress $\sigma_{33} > 0$

$$\left(\frac{\sigma_{33}}{Z_T}\right)^2 = \begin{cases} > 1 \text{ failure} \\ \leq 1 \text{ no failure} \end{cases} \tag{40}$$

Inter-laminar normal stress $\sigma_{33} < 0$

$$\left(\frac{\sigma_{33}}{Z_C}\right)^2 = \begin{cases} > 1 \text{ failure} \\ \leq 1 \text{ no failure} \end{cases} \tag{41}$$

Where: σ_{13} and σ_{23} are the out-of-plane shear stresses, σ_{33} is the stress in the thickness direction (z), and S_T is the transverse shear strength. These failure criteria require reliable estimates of through-thickness stresses and additional strength parameters (Z_T : tensile & Z_C : compressive) and (S_{13} and S_{23}) are in the transverse shear directions.

VI. SIMULATION MODELLING IN COMMERCIAL SOFTWARE PACKAGE

The literature search revealed that majority of the researchers have already utilised the commercial software ABAQUS™/Explicit for the analysis of impact dynamic of composite panels instead of writing time consuming lengthy programs [14] and [15]. The software incorporates a variety of linear and nonlinear shell elements that could accommodate stacks of several plies. Hence, the software was chosen for the present simulations. The numerical simulations based on the test conditions were carried out to predict impact behaviour at ply-level [31]. The same software was selected for simulation modelling to implement drop-weight impact process. The composite panel was meshed with general purpose linear fully integrated quadrilateral conventional shell (S4) 234 elements and reduced integration triangular conventional shell (S3R) 621 elements using two different levels of refinement. Each ply is modelled with deformable one shell element through-the-thickness which behaves according to the continuum damage model. Fine meshes were created in regions where a correct prediction of the damage initiation load is required (impact zone) where damage takes place using the smaller elements allow better simulation of the stress distributions at the mesh-transition regions. In regions away of the impact zone where damage is not expected to occur or its initiation load is not critical course meshes were created. The impactors are modelled by a hardened stainless steel, meshed with fully integrated continuum 8-node C3D8 three-dimensional (3D) linear hexahedral 708 elements. The shank reduces to 10 mm for the ground flat impact face. The round nose shape impactor has radius of 5 mm. Both the impactors have lumped masses equal to the one used in the experiments. Every impact lasted for 1.1 micro-seconds. No catastrophic failures or complete penetrations were assumed. An initial velocity in the vertical direction is prescribed to the impactor, simulating the impact velocity measured during the tests. The drop-weight models were investigated for the range of velocities: 1.6-4.2m/s selected on the basis of the experimental results proposed by James in [20] below. The impactors strike at centre of the laminates. For the given nose profiles (flat & round) of the impactors, it was desired to determine the dynamic response of the plate during impact and to predict ply-by-ply failure as functions of time inside the laminate. Material properties of the simulated laminates were of aerospace grade carbon fibre reinforced as shown in Table 1. Moreover, no catastrophic failures or complete penetrations were assumed. Two models were developed for comparison and verification. Computer generated pre-processed model 1 consists of flat nose impactor as shown in Figure 5(a) and model 2 consists of round nose impactor as shown in Figure 5(b). Impactors were

meshed with reduced integration brick elements while laminates were meshed with sweeping techniques to generate fine mesh (full integration shell elements) under the impactor's contact shape.

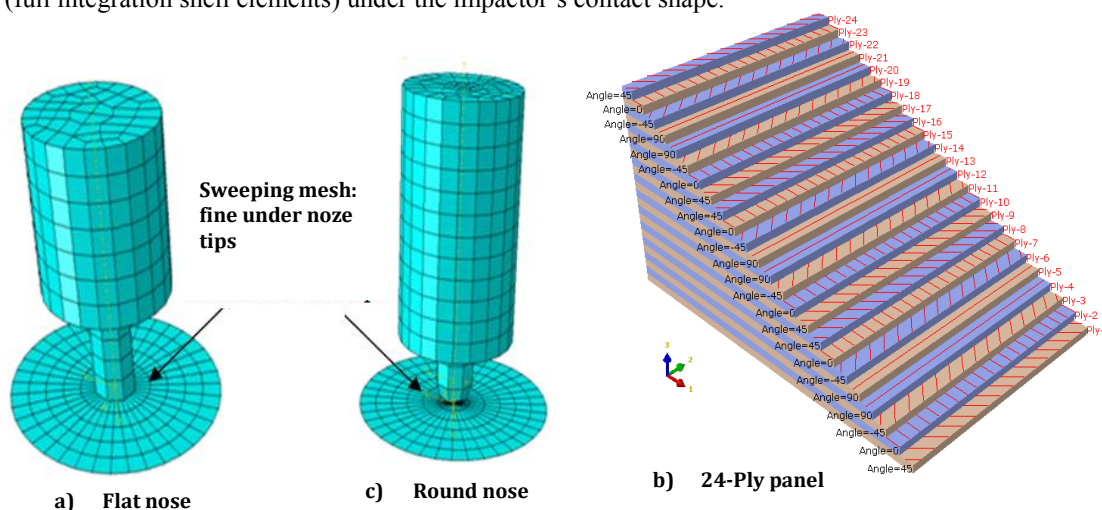


Figure 5: Computer generated meshed models and stack of 24-Ply panel

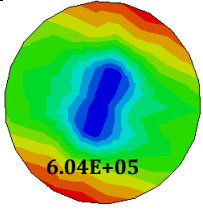
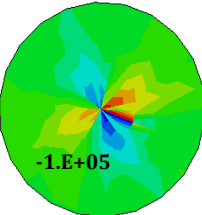
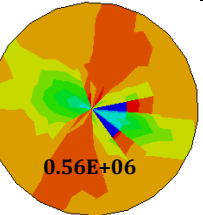
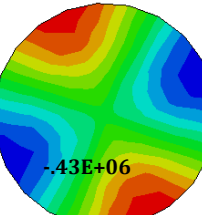
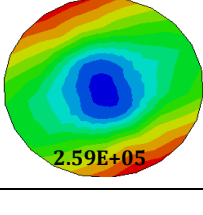
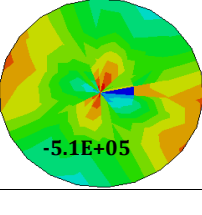
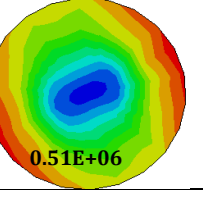
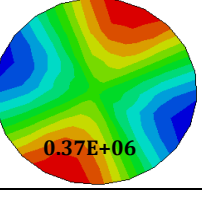
VII. RESULTS AND DISCUSSIONS

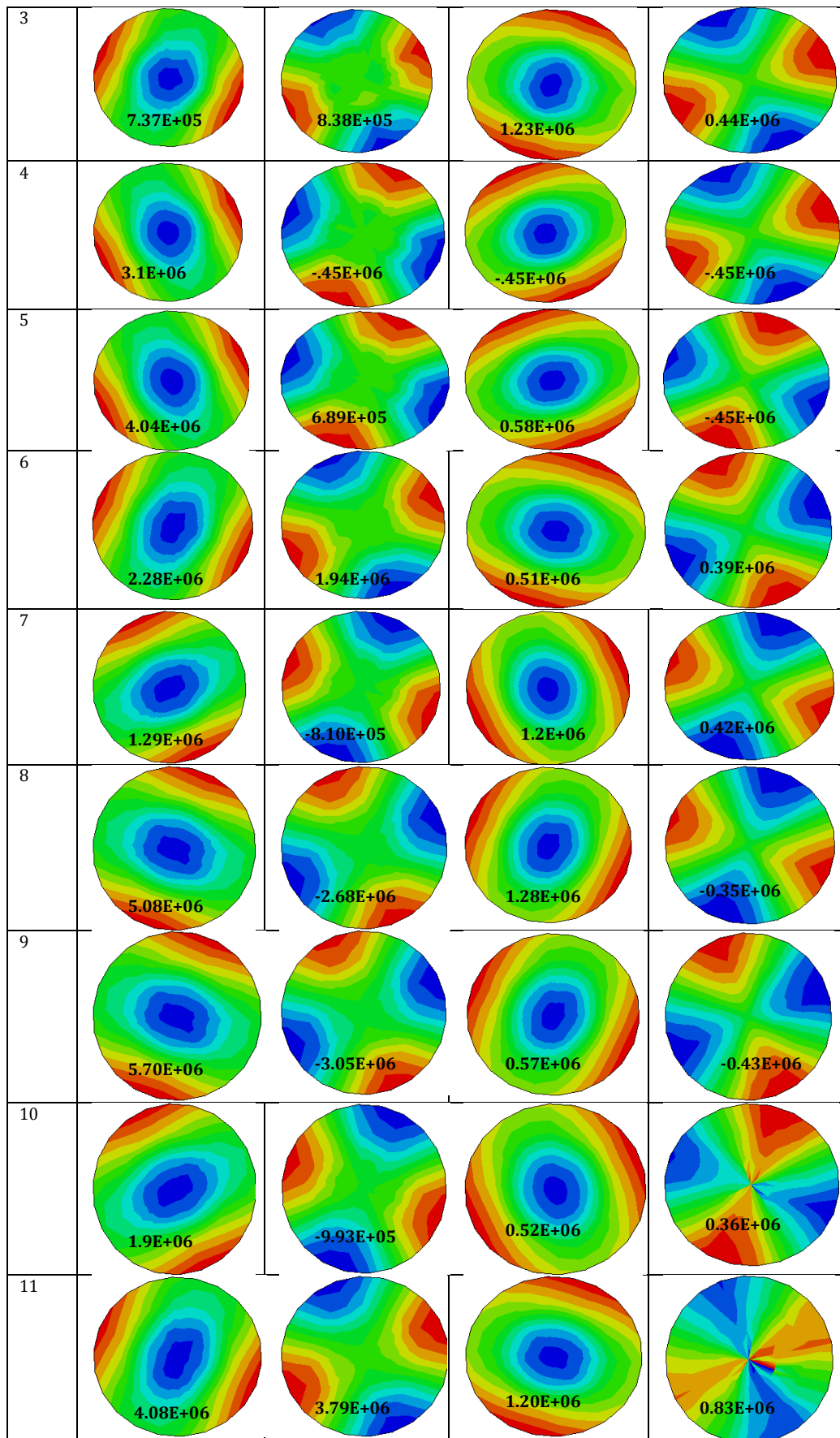
Simulations were performed for 8-, 16-, and 24-Ply panels impacted at velocity range 1.7-4.6m/s. The built-in progressive damage routines for limit (Von Misses), and interactive polynomial (Tsai-Hill & Tsai-Wu) did not exceed allowable limits indicating that the failure criteria predicted no significant damage or ply-level failure as expected. Since simulated panels were relatively thick and ply failures were expected to occur because of higher through-thickness stresses. The limits and polynomial criteria did not utilise through-thickness stresses thus ply failure did not occur. Simulation generated results of relatively thick 24-Ply panels impacted at 4.2m/s were selected for comparisons and discussions utilising through-thickness mode-base failure criteria.

7.1 In-plane and through-thickness stresses based failure criteria

Simulation generated in-plane normal and shear stress quantities were recorded at selected nodes of high stress gradient regions from flat and round nose impacts at 4.2m/s. All contour images and all legend tables show larger value of predicted stress quantities generated from round nose shape impactors as shown in Table 2, Table 3. Stress quantities generated by flat and round nose shape impacts show significant difference among contour images and predicted values of stress quantities. This confirms that round nose impactors generate larger local stresses at and around the impactors' nose tip zones. However, flat nose impactor generates larger damage and stresses are spread all over the global surface of the panel. These stresses quantities would be further utilised to numerically integrate using modified Simpson rule Eq. (42) to compute through-thickness shear stresses.

Table 2: Flat nose with impact velocity 4.2m/s

Ply no	In-plane stress quantities along with simulated panel images			
	S11	S12	S22	S21
1	 6.04E+05	 -1.E+05	 0.56E+06	 -.43E+06
2	 2.59E+05	 -5.1E+05	 0.51E+06	 0.37E+06



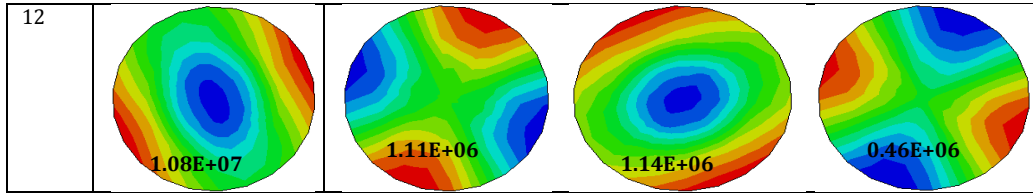
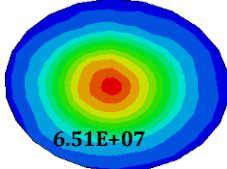
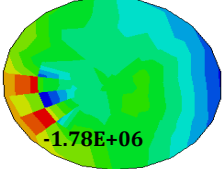
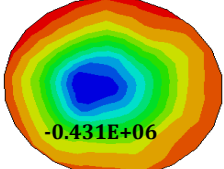
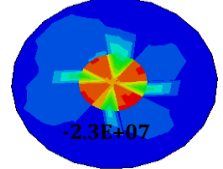
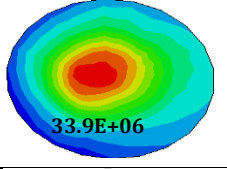
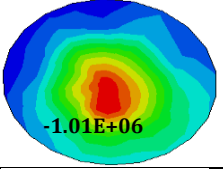
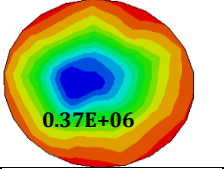
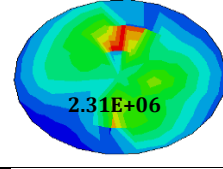
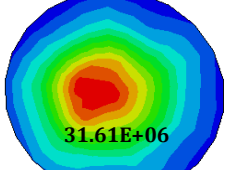
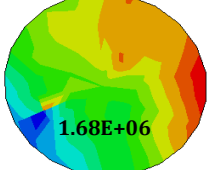
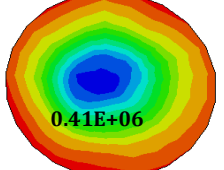
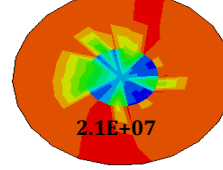
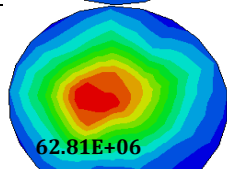
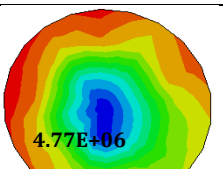
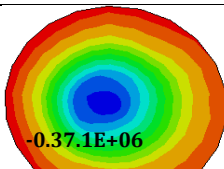
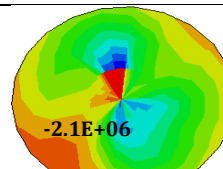
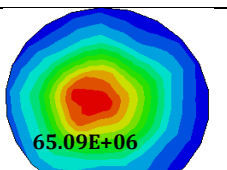
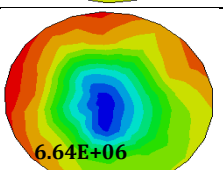
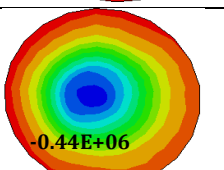
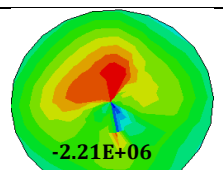
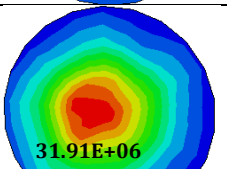
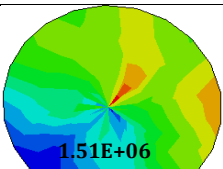
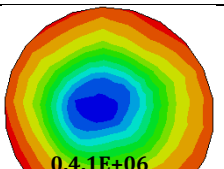
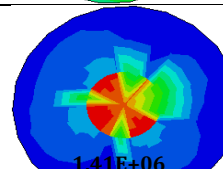
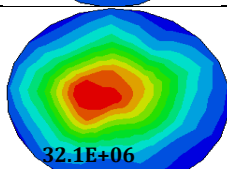
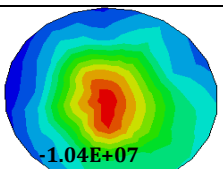
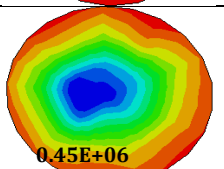
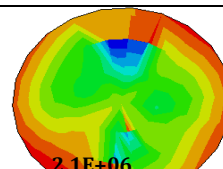
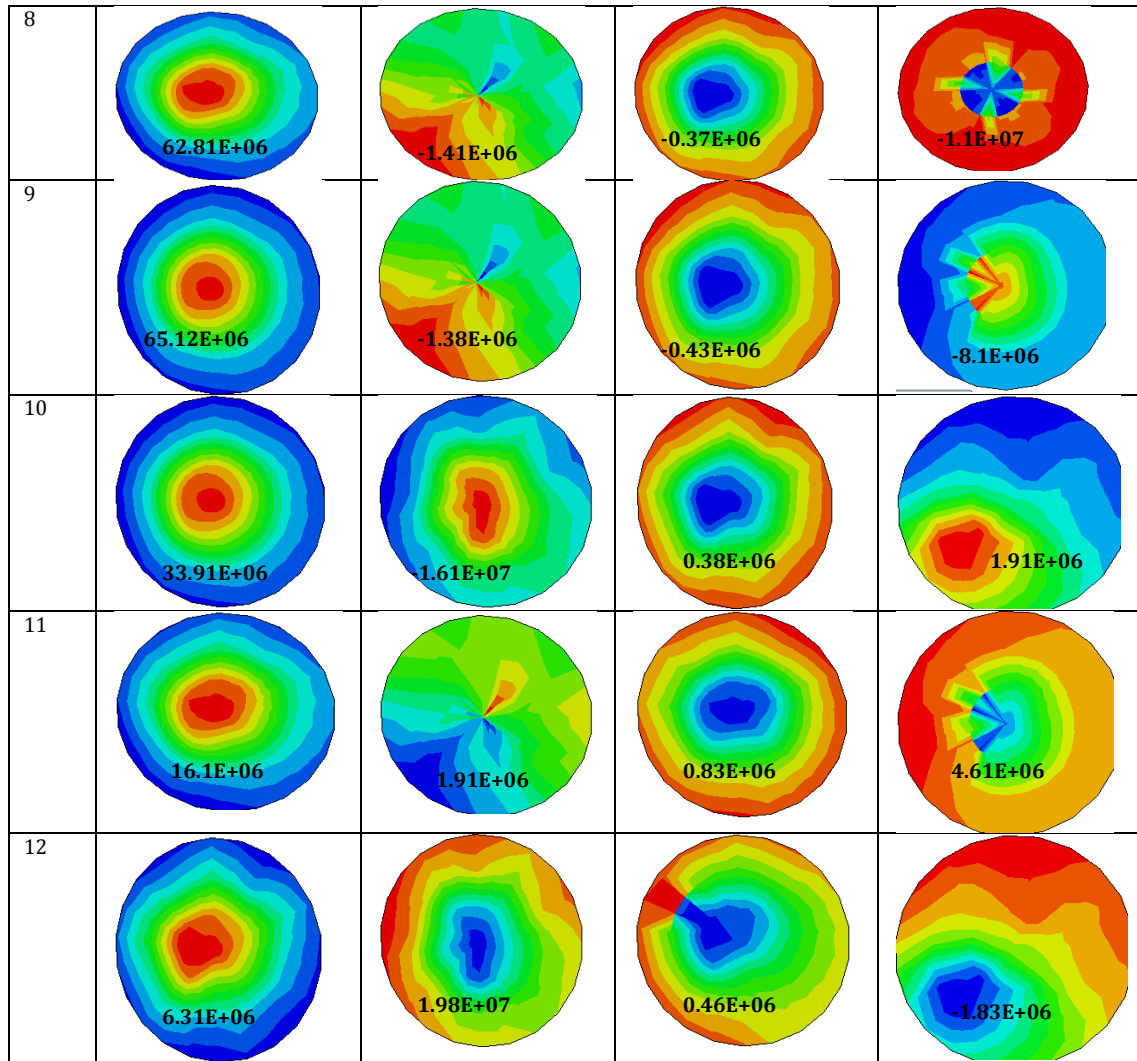


Table 3: Round nose with 4.2m/s

Ply no	In-plane stresses			
	S11	S12	S22	S21
1	 6.51E+07	 -1.78E+06	 -0.431E+06	 -2.3E+07
2	 33.9E+06	 -1.01E+06	 0.37E+06	 2.31E+06
3	 31.61E+06	 1.68E+06	 0.41E+06	 2.1E+07
4	 62.81E+06	 4.77E+06	 -0.37.1E+06	 -2.1E+06
5	 65.09E+06	 6.64E+06	 -0.44E+06	 -2.21E+06
6	 31.91E+06	 1.51E+06	 0.4.1E+06	 1.41E+06
7	 32.1E+06	 -1.04E+07	 0.45E+06	 2.1E+06



The recorded in-plane normal (σ_{11} and σ_{22}) and shear stresses (τ_{12} and τ_{21}) quantities were numerically integrated using modified Simpson’s rule based on second-order polynomial Eq. (42) to predict ply-by-ply through-thickness stresses (τ_{13} and τ_{23}):

$$\int_a^b f(x) dt \approx \frac{h}{3} \left[f(a) + f(b) + 2 \sum_{k=1}^{n/2-1} f(x_{2k}) + 4 \sum_{k=1}^{n/2} f(x_{2k-1}) \right] \tag{42}$$

Where: interval [a, b] is split up in n sub-intervals, with n an even number where equidistant x values are x_0, x_1, \dots, x_n , the step width being $h = \frac{b-a}{n}$.

Table 4: In-plane stresses and tensile-flexural coupling failure criteria

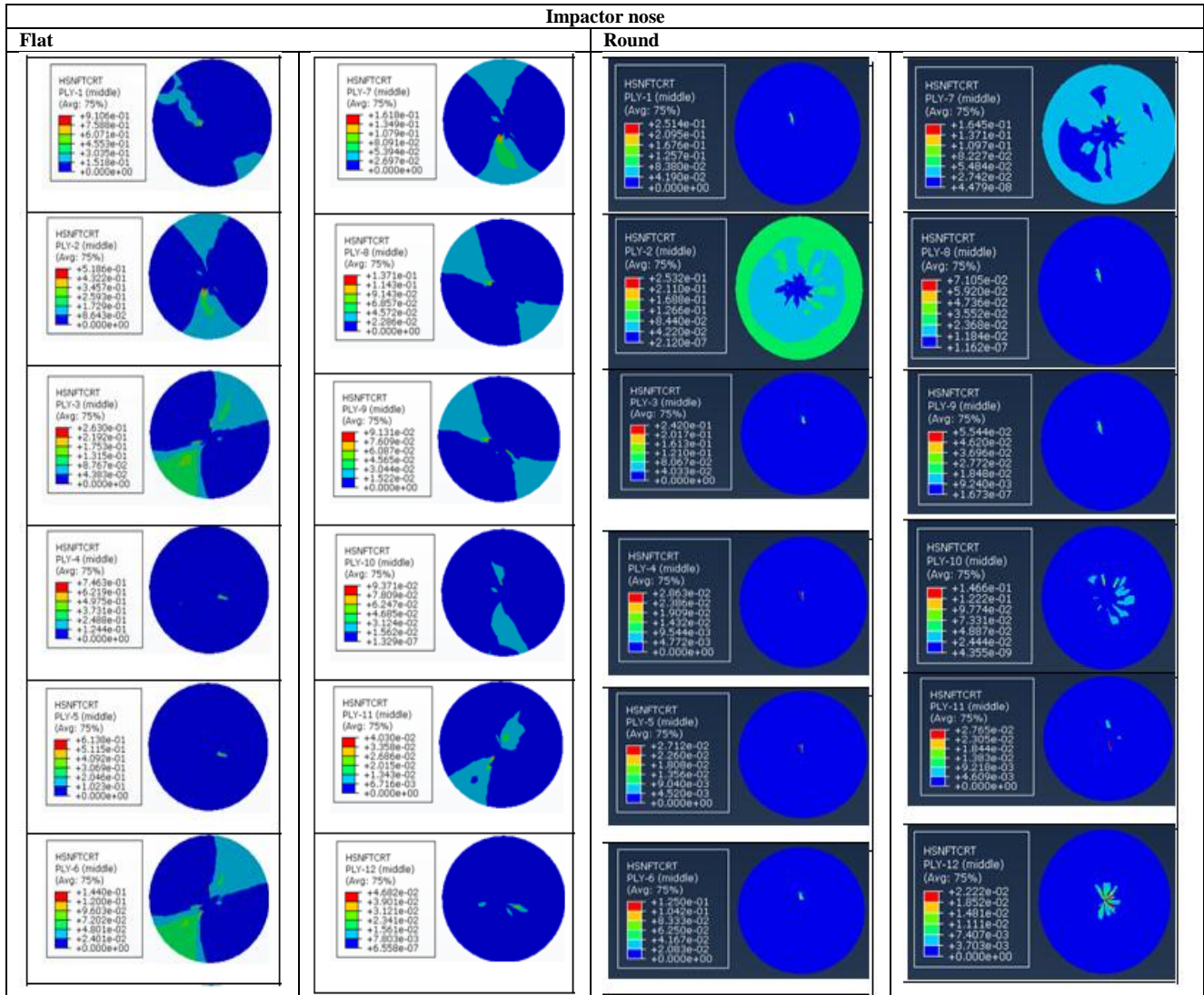
Ply No	Flat Nose			Round Nose		
	In-plane stresses		Tensile-flexural	In-plane stresses		Tensile-flexural
	σ_{11}	τ_{12}	$\left(\frac{\sigma_{11}}{S_T}\right)^2 + \left(\frac{\tau_{12}}{S_{12}}\right)^2 \geq 1$	σ_{11}	τ_{12}	$\left(\frac{\sigma_{11}}{S_T}\right)^2 + \left(\frac{\tau_{12}}{S_{12}}\right)^2 \geq 1$
1	-1.1E+07	-2.8E+05	2.9E-04	4.5E+07	-2.3E+07	2.1E-02
2	-6.0E+06	-4.0E+06	5.7E-04	6.3E+07	2.3E+06	9.6E-03
3	-2.0E+06	1.6E+05	1.0E-05	3.2E+07	2.0E+07	1.4E-02
4	-5.1E+06	3.2E+06	3.8E-04	1.1E+07	-2.2E+06	4.5E-04
5	-4.5E+06	2.9E+06	3.0E-04	1.0E+07	-2.2E+06	3.8E-04
6	-1.4E+06	-2.1E+04	4.5E-06	2.3E+07	1.4E+00	1.2E-03
7	-3.4E+06	-2.1E+06	1.6E-04	3.6E+07	2.1E+06	3.1E-03
8	-4.5E+06	1.4E+05	4.9E-05	2.1E+07	-1.0E+07	4.2E-03
9	-3.5E+06	2.0E+05	3.1E-05	1.7E+07	-8.3E+06	2.9E-03
10	-1.8E+06	-1.00E+06	3.9E-05	1.9E+07	1.92E+06	9.8E-04
11	-3.6E+05	-3.24E+05	3.6E-06	6.1E+06	4.60E+06	7.4E-04
12	-3.37E+04	2.67E+05	2.2E-06	1.77E+06	-1.83E+06	1.1E-04

The components of predicted stresses by flat and round nose impacts at 4.2m/s impact were utilised in tensile-shear coupling, quadratic delamination, and failure criteria Eqs. (32)-(41) to predict possible ply-level damage and failure modes. No failure or severe damage can be seen under columns 3 and 4 using tensile-shear coupling and quadratic delamination criteria as shown in Table 4 while ply no. 8, 9, and 10 failed using quadratic failure criteria as shown in column 7 of Table 5.

Table 5: Through-thickness shear stresses and quadratic delamination failure criteria

Ply No	Flat Nose			Round Nose		
	Through thickness shear stresses		Q Delamination formula	Through thickness shear stresses		Q delamination criteria
	τ_{13}	τ_{23}	$\sqrt{\left(\frac{\tau_{13}}{S_{13}}\right)^2 + \left(\frac{\tau_{23}}{S_{23}}\right)^2} \geq 1$	τ_{13}	τ_{23}	$\sqrt{\left(\frac{\tau_{13}}{S_{13}}\right)^2 + \left(\frac{\tau_{23}}{S_{23}}\right)^2} \geq 1$
1	1.8E+00	-16.84	1.8E-07	-1.1E+06	4.8E+04	1.1E-01
2	2.5E+05	2.51E+05	2.5E-02	-2.4E+06	-2.2E+06	2.4E-01
3	1.1E+03	6.80E+05	1.1E-04	-2.2E+05	-5.3E+06	2.2E-02
4	6.9E+05	-6.89E+05	6.9E-02	-4.8E+06	5.2E+06	4.8E-01
5	8.7E+05	-8.76E+05	8.7E-02	-5.9E+06	6.4E+06	5.9E-01
6	2.4E+03	1.50E+06	2.4E-04	-4.3E+05	-1.0E+07	4.3E-02
7	1.2E+06	1.20E+06	1.2E-01	-8.3E+06	-7.7E+06	8.3E-01
8	1.8E+00	-16.84	1.8E-07	-1.2E+07	5.2E+05	1.2E+00
9	2.0E+06	-3244.63	2.0E-01	-1.3E+07	5.5E+05	1.3E+00
10	1.48E+06	1.47E+06	1.5E-01	-1.1E+07	-9.2E+06	1.1E+00
11	3.55E+03	2.20E+06	3.5E-04	-5.9E+05	-1.4E+07	5.9E-02
12	1.56E+06	-1.60E+06	1.6E-01	-9.6E+06	1.1E+07	9.6E-01

Table 6: Fibre tensile initiation failure criterion: HSNFTCRT



7.2 Failure prediction utilizing software built-in failure criteria

Simulation produced results by flat and round nose impacts at 4.2m/s velocity utilising mode-base failure modes. Failure indices along with legend images from ply 1 to 12 are shown in column 1 and 2 from flat nose impact while from round nose impact in column 3 and 4 of These results matched well to the results in Table 5 that confirmed and validate that results models. Predicted quantities of failure indices most of the plies are greater than one using fibre compression initiation (HSNFCRT) failure mode. Predicted quantities of failure indices for a few plies are greater than one using matrix tensile initiation (HSNMTCRT) failure mode, and using matrix compression initiation (HSNMCCRT) failure mode.

Table 6, Table 7, Table 8, and Table 9. Predicted quantities of failure indices for all plies are less than one using fibre tensile initiation criterion (HSNFTCRT) failure mode. These results matched well to the results in Table 5 that confirmed and validate that results models. Predicted quantities of failure indices most of the plies are greater than one using fibre compression initiation (HSNFCRT) failure mode. Predicted quantities of failure indices for a few plies are greater than one using matrix tensile initiation (HSNMTCRT) failure mode, and using matrix compression initiation (HSNMCCRT) failure mode.

Table 7: Failure prediction using fibre compressive criterion: HSNFCRT

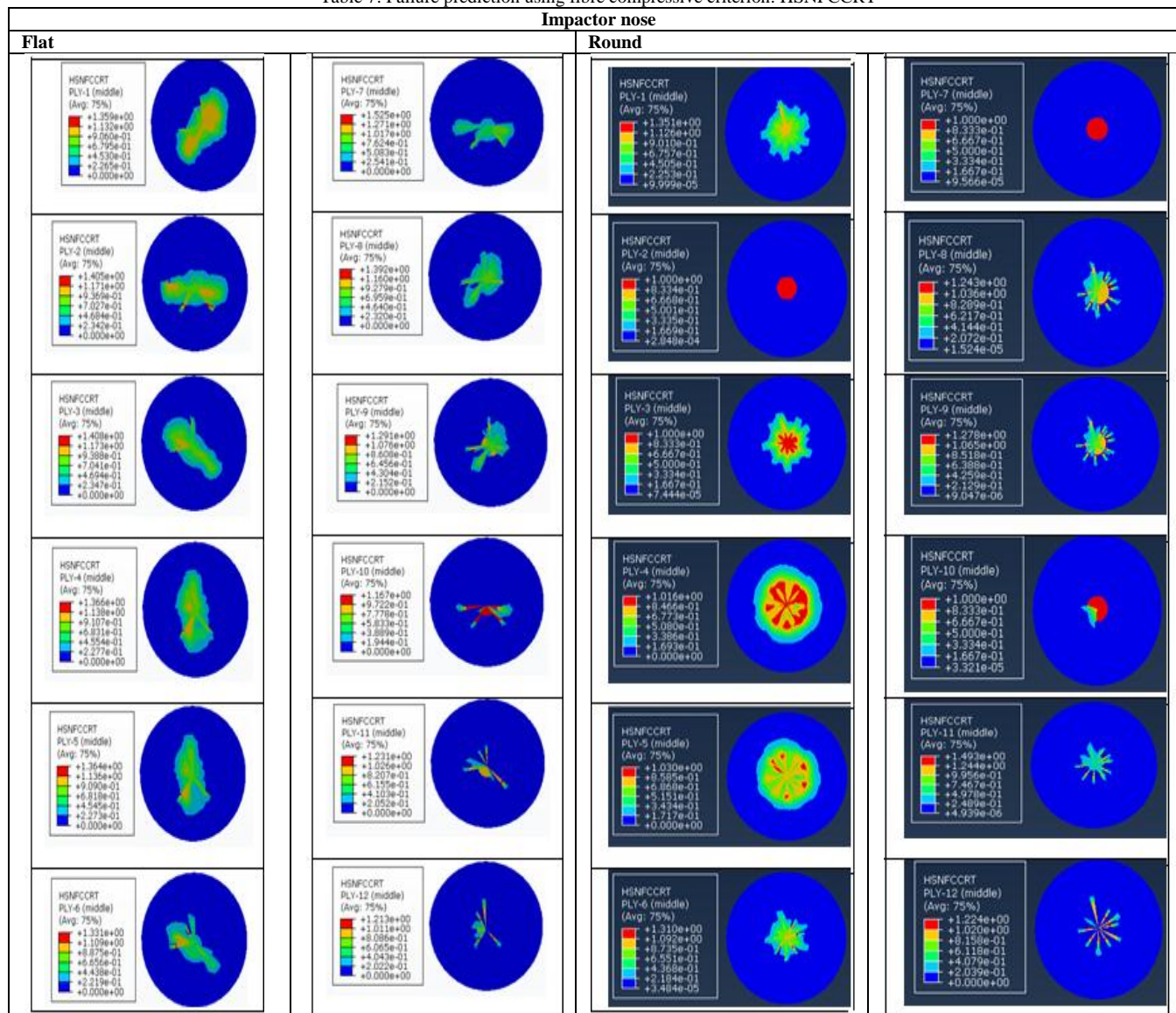


Table 8: Failure prediction using matrix tensile initiation criterion: HSNMTCRT

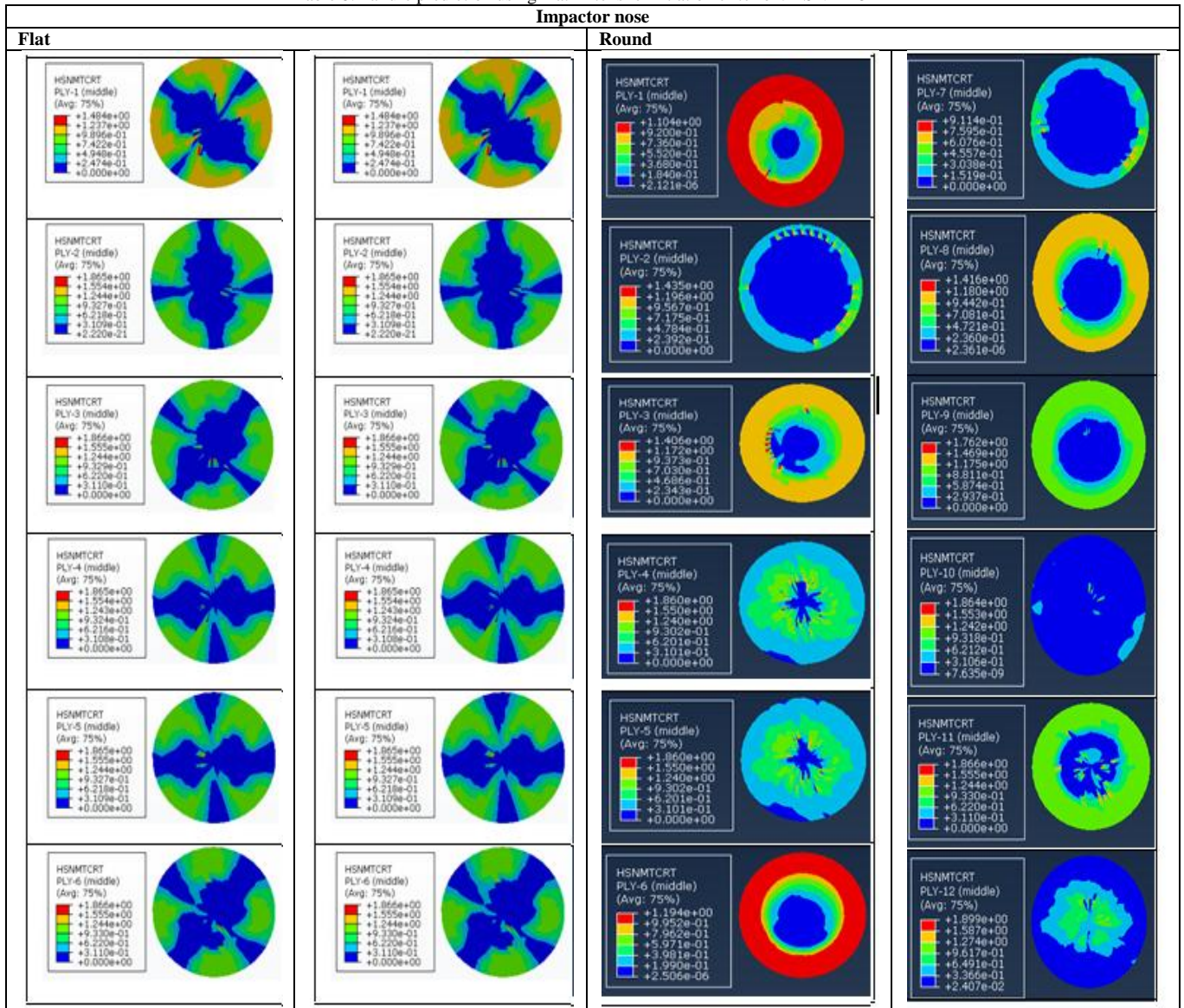
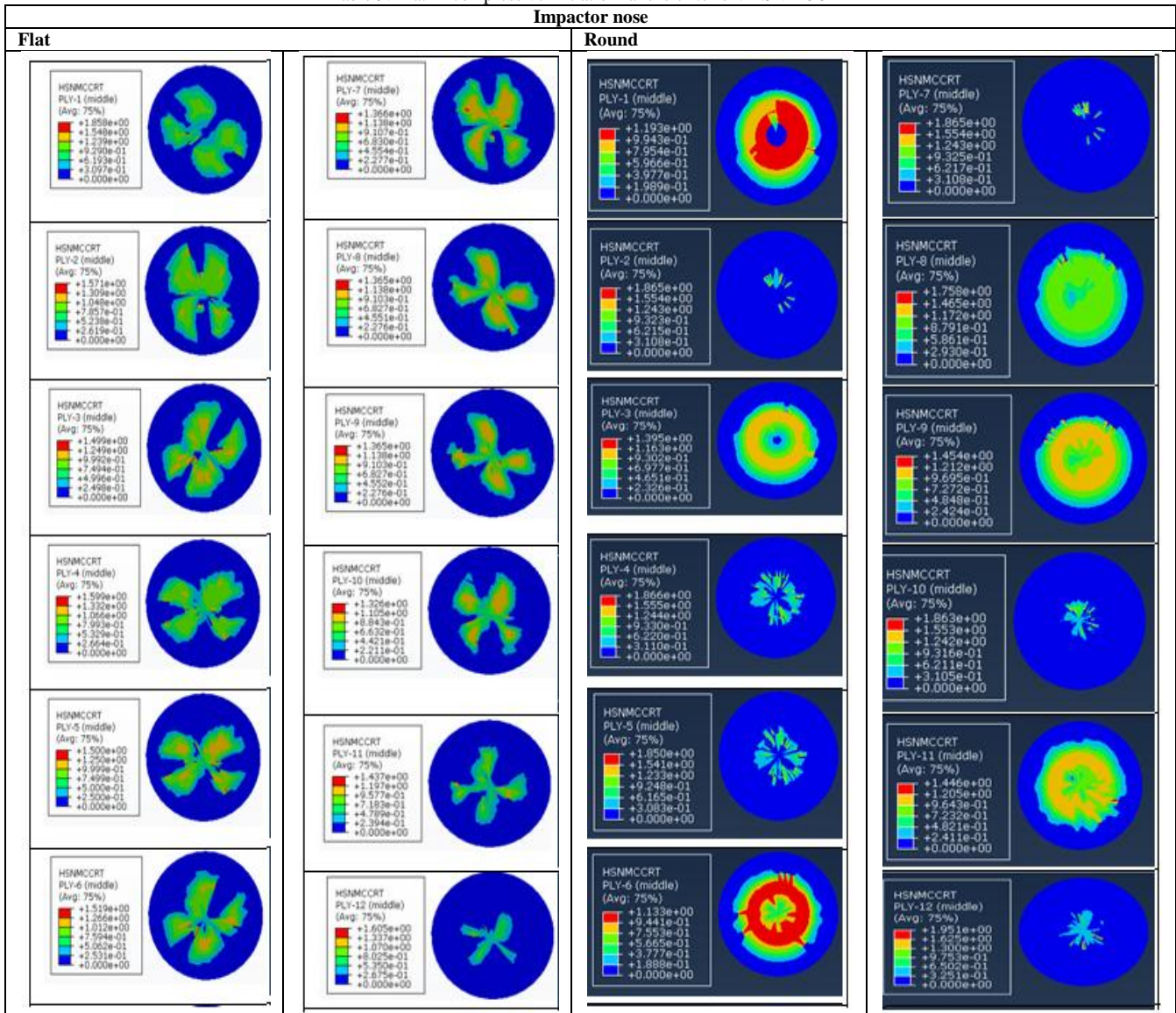


Table 9: Matrix compressive initiation failure criterion: HSNMCRT



VIII. CONCLUSIONS

In this work, simulation models for flat and round nose impacts of composite panels were developed in ABAQUS™/Explicit software to predict ply-level failure and damage. Dynamic responses of 24-Ply panels were predicted along with limit, interactive polynomial, and mode-based failure criteria incorporated as built-in routines. The predicted results were compared to the results available in the literature and found within acceptable range ($\pm 10\%$). Based on consistent comparisons, the following points could be extracted:

- a) The limits and interactive polynomial based failure criteria did not readily predict failed plies or differentiate influence from flat and round nose impacts.
- b) Simulation produced in-plane stresses were utilised to calculate through-thickness stresses. Normal in-plane and through-thickness stresses were utilised in stress-based failure criteria.
- c) Coupling in-plane and out-of-plane stresses criteria predicted severely damaged plies due to round nose impact.
- d) The built-in mode-base Hashin’s failure criteria efficiently predicted ply-level failure and damage.

The study could be useful to complement experimental methods, reduce the number of physical experiments, and simulate similar cases consisting of variety of panels with different material properties, lay-ups, stacking sequences, panel thicknesses, and impactors.

REFERENCES

[1] Oguibe CN and Webb DC. Finite element modelling of the impact response of laminated composite plates. Compos Sci & Technol 1999;59:1913-22.

- [2] Besant T, Davies GAO, and Hitchugs D. Finite element modelling of low-velocity impact response of composite sandwich panels. *Composites Part A* 2001;32:1189-96.
- [3] Kim JK and Kang KW. An analysis of impact force in plain-weave glass/epoxy composite plates subjected to transverse impact. *Compos Sci Technol* 2001;61:135-43.
- [4] Abatan A, Hu H, and Olowokere D. Impact resistance modelling of hybrid laminated composites. *J of Thermoplastics Compose Mater* 1998;11:249-60.
- [5] Sun CT and Liou WJ. Investigation of laminated composite plates under impact dynamic loading using a three-dimensional hybrid stress finite element method. *Compos & Struct* 1989;33:879-84.
- [6] Chandrashekhara K, Okafor AC, and Jiang YP. Estimation of contact force on composite plates using impact-induced strain and neural networks. *Composite Part B* 1998;29:363-70.
- [7] Ramkumar RL and Chen PC. Low-velocity impact response of laminated plates. *AIAA Journal* 1983;21:1448-52.
- [8] Razi H and Kobayashi AS. Delamination in cross-ply laminated composites subjected to low-velocity impact. *AIAA Journal* 1993;31:1498-1502.
- [9] Choi IH and Hong CS. New approach for simple prediction of impact force history on composite laminates. *AIAA Journals* 1994;32:2067-72.
- [10] Pierson MO and Vaziri R. Analytical solution for low-velocity impact response of composite laminates. *AIAA Journals* 1996;34:1633-40.
- [11] Choi HY, Wu HYT, and Chang FT. A new approach towards understanding damage mechanism and mechanics of laminated composites due to low-velocity impact: part II-analysis. *Compos Mater* 1991;25:1012-38.
- [12] Choi HY and Chang FK. A model for predicting damage in graphite/epoxy laminated composites resulting from low-velocity impact. *Compos Mater* 1992;26:2134-69.
- [13] Chung J, Lee JM. A new family of explicit time integration methods for linear and non-linear structural dynamics. *Int J Numer Methods Eng* 1994;37:3961-76.
- [14] Hulbert GM, Chung J. Explicit time integration algorithms for structural dynamics with optimal numerical dissipation. *Comput Meth Appl Mech Eng* 1996;137:175-88.
- [15] Chang SY, Liao WI. An unconditionally stable explicit method for structural dynamics. *J Earthquake Eng* 2005;9:349-70.
- [16] Noh G, Ham S, Bathe KJ. Performance of an implicit time integration scheme in the analysis of wave propagations. *Comput Struct* 2013;123:93-105.
- [17] Payen DJ, Bathe KJ. A stress improvement procedure. *Comput Struct* 2012;112 113:311-26.
- [18] Kim J, Bathe KJ. The finite element method enriched by interpolation covers. *Comput Struct* 2013;116:35-49.
- [19] Idesman AV, Foley JR. Accurate finite element modelling of linear elasto-dynamics problems with the reduced dispersion error. *Comput Mech* 2011;47:555-72.
- [20] James RA. Impact damage resistance and damage tolerance of fibre reinforced laminated composites. PhD Thesis, University of Bolton, UK, 2006.
- [21] Farooq U, Myler P. Efficient computational modelling of carbon fibre reinforced laminated composite panels subjected to low-velocity drop-weight impact. *Mater Des* 2014;54:43-56.
- [22] Schoeppner GA, Abrate S. Delamination threshold loads for low-velocity impact on composite laminates. *Compos Part A Appl Sci Manuf* 2000;31:903-15.
- [23] Davies GAO, Zhang X. Impact damage prediction in carbon composite structures. *Int J Impact Eng* 1995;16:149-70.
- [24] Abrate S. *Impact on composite structures*. Cambridge University Press: Cambridge 2005.
- [25] Bathe KJ, Noh G. Insight into an implicit time integration scheme for structural Dynamics. *Comput Struct* 2012;98-99:1-6.
- [26] Rio G, Soive A, Grolleau V. Comparative study of numerical explicit time integration algorithms. *Adv Eng Software* 2005;35:252-65.
- [27] Nsiampa N, Ponthot J, Noels L. Comparative study of numerical explicit schemes for impact problems. *Int J Impact Eng* 2008;35:1688-94.
- [28] Zhang X. Impact damage in composite aircraft structures – experimental testing and numerical simulation. *Journal of Aerospace Engg* 1998;212(4):45-259.
- [29] Hashin Z. Failure criteria for unidirectional fibre composites. *J Appl Mech* 1980;47:329-334.
- [30] Farooq U, Myler P. Damage and energy absorption behaviour of low-velocity impacted fibre-reinforced composite panels using analytical and data filtering techniques. *Int J Rec Res Appl Sciences*: 21021;8(4):13-27.
- [31] Farooq U, Myler P. Stress base modelling and computer simulation of drop-weight impact response of composite panels with domain partitioning and adaptive meshing techniques. *Int J Rec Res Appl Sciences*: 2021;8(4):38-58
- [32] Tsai WS, Melo JDD. *Composite Materials Design and Testing—Unlocking mystery with invariants*. Stanford, USA: DEStech Publications, Inc; 2015.
- [33] Chiu LNS, Falzon BG, Chen B, Yan W. Validation of a 3D damage model for predicting the response of composite structures under crushing loads. *Compos Struct*, 2016;147:65-73.

Corresponding author: Umar Farooq

Emails: adalzai3@yahoo.co.uk and u.farooq@bolton.ac.uk

Address: C/O Professor Dr Peter Myler

Head of Engineering and Design Department,

University of Bolton, Bolton BL3 5AB UK

Phone and fax: 01204 903011